Publication III

Manuscript reprinted from Progress in Photovoltaics 14(2006), p. 213-224

Identification of degradation mechanisms in field-tested CdTe modules

Thomas Carlsson, Andy Brinkman

Abstract

Field tests and accelerated ageing tests were conducted on CdTe photovoltaic modules with Sb-based back contacts. Significant performance degradation was observed during one and a half years of outdoor exposure. Small-area samples were prepared from field tested modules and characterized with current-voltage, capacitance-voltage and resistance measurements. Results show that module performance degraded in the field at least partly because of a decrease in doping concentration close to the CdS/CdTe junction and an increased resistance in the transparent front contact. A comparison to results in the literature indicates that bias voltage may play a role in the degradation process.

Keywords: photovoltaics, CdTe, field test, accelerated ageing, degradation

1. Introduction

Polycrystalline CdTe thin-film technology has recently emerged as a viable competitor to the silicon-based technologies which dominate the photovoltaic market today. One of the most important requirements new technologies have to demonstrate is proven long-term stability, which in the case of thin-film technologies depends on the cell material as well as on the interconnects between the individual cells and on the protective encapsulation material [1]. The stability of CdTe cells is a complex problem which depends to a great degree on cell structure. The main stability issue for CdTe cells is the non-ohmic back contact, and stability improvements at the cell level have focused primarily on finding stable contacts without sacrificing efficiency. In accelerated ageing tests, Cu diffusion has been identified as a degradation mechanism in cells with copper-containing back contacts, and humidity has been identified as a severe stress factor due to its role in the formation of a back-contact barrier [2-4]. In addition to the back contact issues, impurity diffusion and changes in doping profiles may affect cell stability [5,6]. Results from field tests lasting up to 3 years have in general shown stable performance [7-9], but field experience is limited in its geographical scope and few results have been reported for modules utilizing new cell structures.

In order to verify and improve the stability of CdTe modules with different cell structures, more detailed information on the degradation modes which occur in outdoor use in different climates needs to be obtained, so that results from accelerated ageing tests can be correlated better with field test results [10]. In this paper, a methodology for identification of degradation modes in field-tested CdTe modules is presented, and a comparison is made between accelerated ageing experiments and field test results for CdTe modules with Sb_2Te_3 back contacts. Small-area samples are prepared from modules whose output power degraded by more than 10% during one and a half years of outdoor exposure in southern Finland. The analysis of small samples shows that module degradation in the field manifests itself as a decrease in fill factor accompanied by decreasing rollover at far forward bias. The degradation mechanisms causing this behaviour in the samples are identified as i) decreased doping density at the junction, ii)

increased series resistance in the transparent front contact, and iii) increased shunt conductance in the cell material and through one interconnect. The modules studied in this paper were tested in the field during the first phase of the EU project PYTHAGORAS (ENK5-CT-2000-00334) [11].

2. Experimental

2.1. Sample description

All CdTe modules studied in this work were from a pilot production line and had the following cell structure: glass/ITO/SnO_2/CdS/CdTe/Sb_2Te_3/NiV. In damp heat testing, mini-modules 10cm•10cm in size were used, while field tested modules were 60cm•120cm in size.

2.2. Damp heat tests

Damp heat tests were performed on two mini-modules according to the IEC standard 61646 at a temperature of 85^{o}C and a relative humidity of 85% for slightly over 1000h in an Arctest ARC-400 climate chamber. One of the mini-modules (hereafter referred to as D1) was unencapsulated, while the other one (D2) was encapsulated with EVA.

2.3. Field tests

In the field test phase from October 2001 to June 2003, 16 large modules were deployed at the Helsinki University of Technology testsite (location N 60^{o}11', E 24^{o}49'). Modules were tilted at an angle of 45^o due south. Module IV-curves and the plane-of-array (POA) irradiance at the beginning of IV-scanning were recorded at 10 minute intervals while module temperatures and global and diffuse horizontal irradiance (GHI and DHI) were measured every 10 seconds and stored as five minute averages. The modules were maintained in open circuit at all times except during IV-scanning. Within the PYTHAGORAS project, the same measurements were also carried out in Germany and in Spain [11].

2.4. Selection and preparation of small-area samples from field modules

Two modules with significant performance degradation in the field tests, hereafter referred to as modules F1 and F2, and a reference module REF which had not been deployed outdoors, were chosen for detailed studies. The short-circuit currents (I_{SC}), open-circuit voltages (V_{OC}) and fill factors (FF) of the three modules were measured with a solar simulator before the field tests, and differed from each other by 2–5%. To make REF a more precise reference for the undegraded performance of F1 and F2, scaling factors of the form $S_F = Y_{REF}/Y_F$, where S_F is the scaling factor, Y is a general symbol for a performance parameter and the subscript F refers to F1 or F2, were calculated from the simulator results. The I_{SC}, V_{OC} and FF values from the measured IV-curves were multiplied by the scaling factors before comparison (see section 3.3.2). Nine samples 20mm•25mm in size were cut from each module with a tile cutter. Each sample included a cell area with interconnect scribe lines on both sides. To obtain the samples, three strips were cut from each module, one at the middle of the 120cm long

face of the module and the two others 30 cm above and below the middle, respectively. From each strip, one sample was cut from the middle and two from the opposing edges. The samples were polished on a SiC grinding pad to remove the backside glass. After nearly all the glass had been polished off, the encapsulation film was peeled off by hand, leaving the CdTe cell structure below the film unharmed. To facilitate electrical characterization of the samples, a 10mm wide active region was defined with a scalpel and the rest of the CdTe/CdS film was scraped off to reveal the transparent front contact. The length of the active region was approximately 8.5mm, and it was flanked on both sides by the interconnects.

2.5. Measurement methodology for separation of degradation modes

In order to distinguish between the effect of different degradation modes on the performance degradation of modules F1 and F2, the IV-characterization of the samples was performed in three different ways. The primary objective was to separate the effect of degradation in the interconnect structures from the degradation in the active cell material. A basic interconnect structure for a superstrate CdTe module is shown in the top right corner of Figure 1. It contains three scribe lines (running perpendicular to the figure plane).

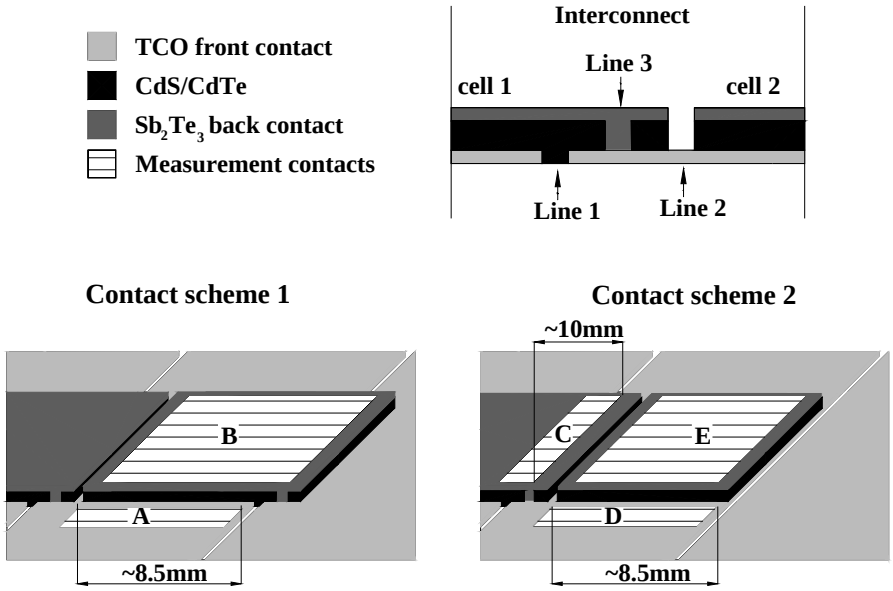

Figure 1. *Interconnect structure with scribe lines indicated and contacting schemes for electrical characterization of samples with and without interconnects (not drawn to scale). Measurement contact areas indicate area covered by silver conducting paint.*

Line 1 separates the front contacts of cells 1 and 2 from each other, and line 2 separates the back contacts. Line 3 connects the back contact of cell 1 to the front contact of cell 2. The potential interconnect degradation modes are (at line 1) decreased shunt resistance at the front contact separation scribe (**R_{SH}**, degradation modes are designated with bold letters), increased series resistance at the exposed part of the front contact (at line 2), and increased series resistance at the interface between the transparent conducting oxide (TCO) and the back contact material (at line 3). In this study, the latter

two could not be studied separately and were therefore lumped together as one degradation mode ($\mathbf{R_{TCO/back}}$). The remaining degradation modes in a module are increased series resistance in the back and front contacts ($\mathbf{R_{TCO}}$, $\mathbf{R_{back}}$) and degradation in the active material (**Cell**).

To separate the effect of different degradation modes from each other, silver conducting paint was painted over copper tape strips to create measurement contacts according to the schemes shown in Figure 1, where the striped areas correspond to the area covered by the paint. The measured active area was 10mm•8.5mm in every measurement. IV-curves were first measured with the shunt interconnect (contact scheme 1, contacts A and B), after which the A and B measurement contacts were wiped off with acetone and the shunt interconnect was removed with a scalpel. The sample was then contacted again and measured over the active area without either shunt or series resistance losses (scheme 2, contacts D and E) and with the series interconnection (scheme 2, contacts C and E). The degradation modes which influence each measurement are shown in Table 1. These three measurements allowed changes in $\mathbf{R_{SH}}$ and $\mathbf{R_{TCO/back}}$ to be separated and quantified by cross-comparison. Changes in $\mathbf{R_{TCO}}$ could be identified with a separate resistance measurement on the TCO surface, and this allowed the identification of **Cell** degradation effects from the D-E IV-measurement. $\mathbf{R_{back}}$ could not be distinguished with the contact schemes used here. The current collection geometry of contacts A and D was different from that of C since the length of the active region was 8.5 mm and the width 10mm.

***Table 1**: Degradation modes affecting the measurement from different contacts.*

Contacts	Degradation modes
A-B	$\mathbf{R_{TCO}}$, **Cell** and $\mathbf{R_{SH}}$
C-E	$\mathbf{R_{TCO}}$,**Cell** and $\mathbf{R_{TCO/back}}$
D-E	$\mathbf{R_{TCO}}$ and **Cell**

2.6. Sample characterization

IV-curves were measured with a Keithley 2420 SourceMeter under 1000 W/m^2 illumination in a solar simulator. Mini-modules D1 and D2 were measured at a module temperature of 40^{o}C, while the small samples were attached to a platform whose temperature was kept at 25^{o}C with a Peltier element. Capacitance-voltage (CV) measurements were performed at room temperature in the dark with a Zahner IM6 Electrochemical Workstation. The measurement frequency was 100 kHz.

3. Results

3.1. Damp heat tests

Damp heat tests were conducted for a total of 1032 hours. Figure 2 shows the "cell-level" IV-curves of mini-modules D1 and D2 in the beginning of the test and after 1032h of accelerated ageing. Cell-level curves were calculated by dividing module

voltage with the number of cells in the module, and dividing module current with the unit cell area. It can be seen in Figure 2 that neither module degraded at all during the test, D1 shows a slight increase in V_{OC} and D2 an increase in FF after the test. The CdTe cell structure of the modules studied here is thus extremely tolerant to both heat and humidity in the dark. Since no degradation was detected in modules D1 and D2, no further studies were conducted on them.

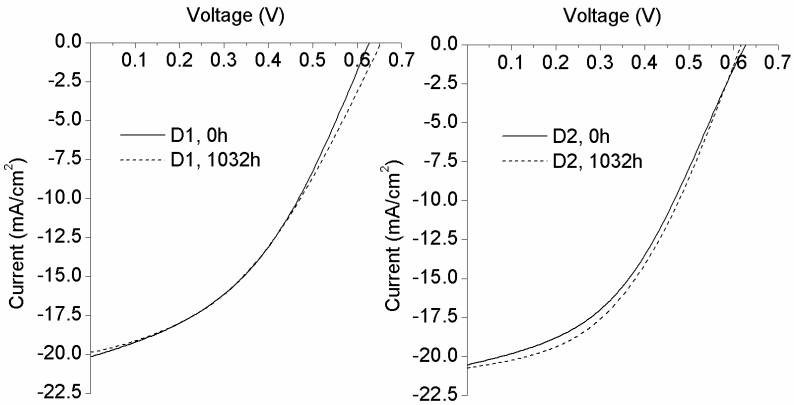

Figure 2. *Cell-level IV-curves for mini-modules D1 and D2 before and after damp-heat test.*

3.2. Field tests

Performance degradation during the field test was quantified by analysing the data measured at a POA irradiance of 800 W/m^2, since the standard test irradiance of 1000 W/m^2 occurs rarely in Finland. To include enough data for calculating reliable averages, all IV-scans conducted within the interval 780 – 820 W/m^2 were included in the calculations. The irradiance dependence of the performance parameters I_{SC} and maximum power point current (I_{MPP}) was taken into account by multiplying each value with a factor of (800 W/m^2) / (POA irradiance), while V_{OC} and maximum power point voltage (V_{MPP}) were assumed to be independent of irradiance within the selected irradiance interval. To improve the quality of the data, I_{SC} and I_{MPP} values were taken only from IV-scans during which GHI/DHI > 4.5. V_{OC} and V_{MPP} values were found to be independent of the GHI/DHI ratio at high POA irradiances, and were therefore not subjected to that filtering condition. A temperature correction to a reference temperature of 40^{o}C was calculated for each measured parameter.

From this data set, weekly averages of the temperature- and irradiance-corrected performance parameters V_{OC}, V_{MPP}, I_{SC}, I_{MPP}, FF and maximum power (P_{MPP}) were calculated. Figure 3 shows the development of the weekly averages of the four primary parameters during the test period as an average over all 16 modules, and separately for modules F1 and F2. The averages have been normalized to their maximum value during

the test period. From Figure 3, it can be seen that the average maximum power degradation was 12–13% from June 2002 to June 2003. Module F1 degraded slightly less (10–12%), while module F2 shows the same amount of degradation as the average module. Although the maximum values of different performance parameters occurred at different times, the degradation in output power can be attributed firstly to a decrease in FF (9% for the average module and for module F2, 7% for module F1) and secondly to a decline in V_{OC} (6% for the average module and module F2, 4.5% for module F1). I_{SC} data shows a lot of scattering due to the irradiance sensitivity of I_{SC}, and no clear pattern of degradation can be distinguished. In the corresponding field tests conducted in Germany and Spain, no signs of performance degradation were observed during the same one year period.

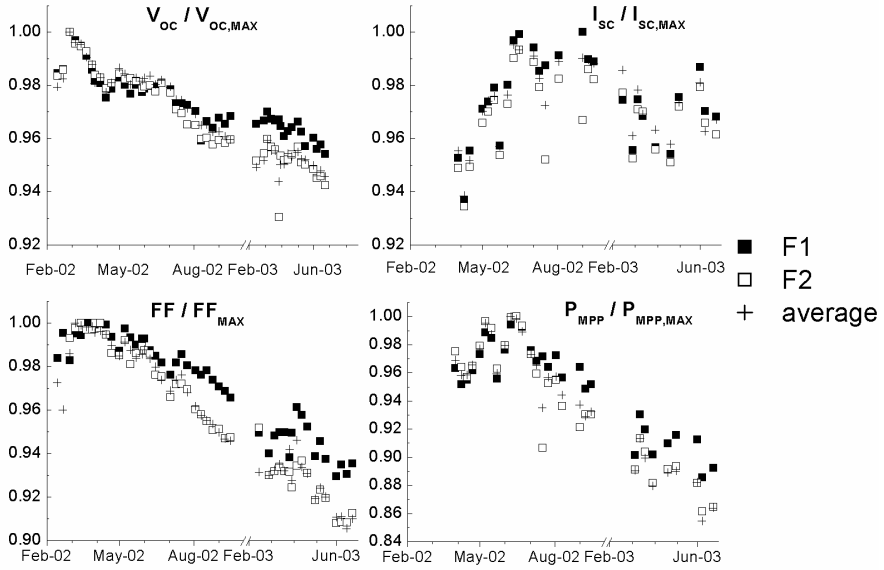

Figure 3. *Normalized weekly averages of temperature- and irradiance-corrected module performance parameters in the POA irradiance interval 780-820 W/m^2 shown as an average calculated over all 16 modules and for modules F1 and F2 separately.*

3.3. Analysis of samples from field modules

General differences between the IV-curves from the prepared small samples and the large modules determine which symptoms of module degradation can be distinguished from the small sample IV-curves. Figure 4 shows the IV-curve of a typical 1cm•1cm sample from module REF (this sample will be referred to as R1 below to distinguish it from the entire module REF), measured from contacts D-E in the simulator at 1000 W/m^2 irradiance. Also shown in Figure 4 is a typical cell-level IV-curve measured in the field from module F1 in June 2002 at the same irradiance. The following conclusions can be drawn:

1. The largest difference between the IV-curves is in the current, I_{SC} being 24.5 mA/cm^2 for R1 and 16.2 mA/cm^2 for F1. This difference may be due to current mismatch between cells and large-area effects such as nonuniformity in the active

layers, and since such factors can not be taken into account in this study, it is suggested that degradation mechanisms which would contribute to loss of current in a large module would not necessarily be apparent in the small sample measurements.

2. The V_{OC} of module F1 (0.594V) is less than that of R1 (0.657V). Two factors explain this difference: the outdoor IV-curve of F1 was measured at a module temperature of 50°C while the simulator IV-curve was measured at 25°C. Correcting the voltage of R1 to a temperature of 50°C brings it down to approximately 0.62V. More importantly, the calculated cell-level voltage of a large module corresponds to the average cell voltage, and each individual cell voltage is determined by the weakest point in that particular cell. Therefore, reliable detection of degradation in module V_{OC} from small samples is likely to require a larger sample set than the one used in this study.

3. The FF is smaller for R1 (41.2%) than for F1 (43.8%). Unless the shunt resistance varies markedly across the cell area (which would also manifest itself as a low value for V_{OC}), the fill factor is determined by the cell characteristics across the whole area. Small-sample FF results can thus be considered reliable indicators of degradation in module FF if the V_{OC} values of the studied sample and a reference sample are comparable.

4. The R1 IV-curve shows rollover behaviour at far forward bias, and the same phenomenon is also visible close to V_{OC} in the F1 IV-curve. Rollover is a common characteristic in CdTe cells related to the presence of a reverse-biased back contact diode [12,13], and in this study it is a characteristic of all measured samples.

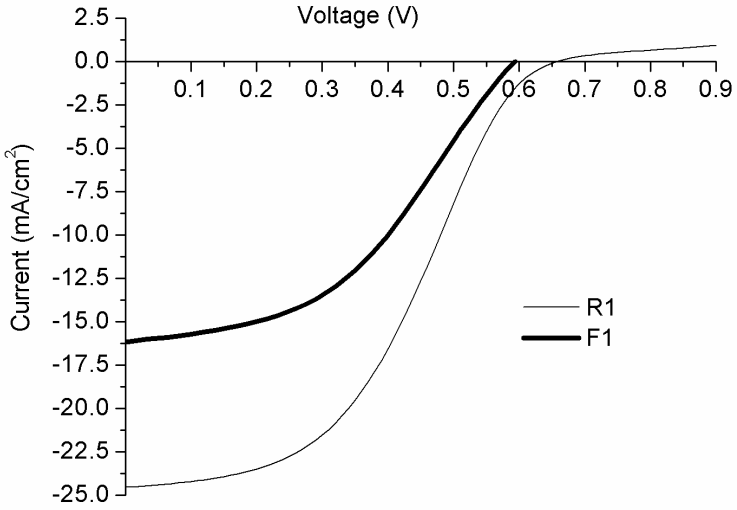

Figure 4. *Comparison between a cell-level IV-curve from module F1 (60cm•120cm) measured in the field and a simulator-measured IV-curve from sample R1 (1cm•1cm), both at 1000 W/m² irradiance.*

3.3.1. Evaluation of interconnect degradation

Of the original 9 samples from each module, 6 samples from module F1, 6 from module F2 and 7 from module REF were unharmed after the cutting and polishing phases of sample preparation. Light IV-curves were measured from –0.4V to +0.9V for each sample separately, and an average curve was then calculated for all three modules. Figure 5 shows the average IV-curves for samples from modules F1 and F2 in the first and fourth quadrants measured from contact pairs A-B, C-E and D-E. The A-B curve deviates from the two others in the first quadrant, which may be an indication of shunting through scribe line 1. However, in the fourth quadrant all three IV-curves very nearly overlap for both modules, so the effect of the shunt on cell performance appears to be negligible.

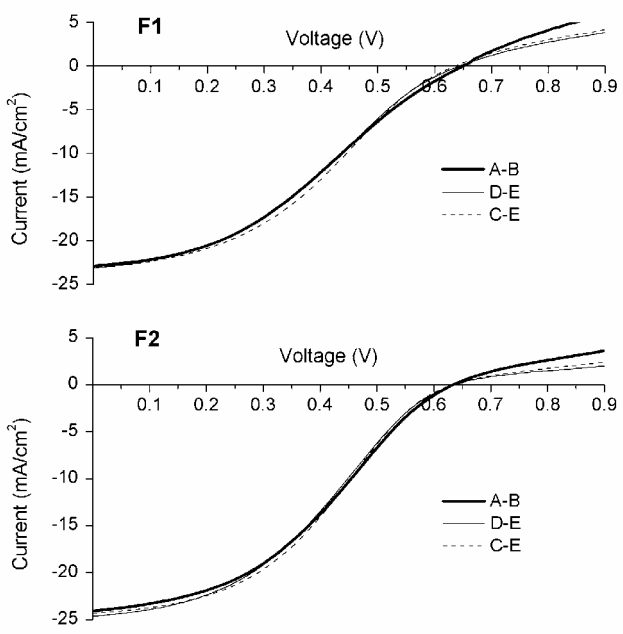

Figure 5. *Average sample IV-curves from modules F1 and F2 measured with the three different contacting schemes presented in Figure 1. For both modules all three curves nearly overlap, which indicates that the cell interconnects have not degraded significantly.*

3.3.2. Evaluation of cell degradation

Since no significant interconnect degradation was observed, the explanation for module degradation was expected to be found in the active area measurements from contacts D-E which were influenced only by degradation modes $\mathbf{R_{TCO}}$ and **Cell**. Figure 6 shows the average sample IV-curves measured from contacts D-E for each module. Table 2 shows the performance parameters from these curves after the F1 and F2 parameters had been scaled to enable direct comparison to REF (see section 2.4). Standard deviation between samples is presented as an error estimate. Referring to the discussion given earlier, it is unlikely that the lower I_{SC} of the F1 samples would have influenced module current in the field, and differences in V_{OC} are too small to indicate that the degradation

mechanism leading to V_{OC} degradation in the field can be identified from this sample set. Fill factor degradation, on the other hand, is expected to be symptomatic of the degradation observed in the field.

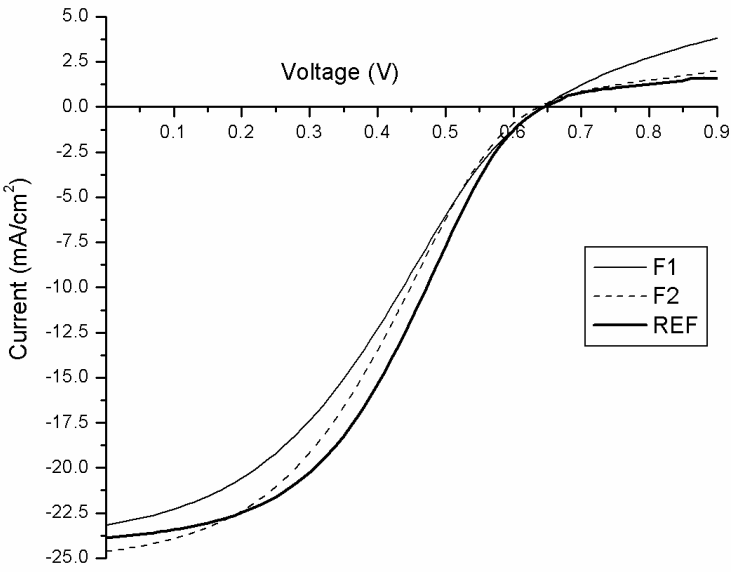

Figure 6. *Average sample IV-curves measured from contacts D-E for all three modules. Both field-deployed modules F1 and F2 show a decrease in P_{MPP} and FF. The decrease in rollover is more pronounced for module F1.*

Table 2*: Key performance parameters from Figure 6. The parameters of F1 and F2 have been multiplied with the corresponding scaling factor S_F. Error estimates were calculated from the standard deviation over all samples.*

Module	I_{SC} (mA/cm^2)	V_{OC} (V)	FF (%)
F1	22.2 ± 0.9	0.63 ± 0.04	37.5 ± 5.0
F2	24.1 ± 1.8	0.62 ± 0.01	39.0 ± 1.8
REF	23.9 ± 1.2	0.64 ± 0.02	41.3 ± 2.9

It is seen in Figure 6 that degradation in FF is accompanied by a decrease in rollover at forward bias in both F1 and F2. This change in IV-characteristics corresponds closely with the results from accelerated ageing tests presented in [6] for cells with a different structure. In a more detailed analysis of the IV-characteristics measured from contacts D-E, dI/dV was calculated as a function of voltage for each sample, and the average is plotted in Figure 7. dI/dV at far reverse bias gives an estimate for the shunt conductance. Since the data shows a sloping trend, only upper limits for the shunt conductance can be determined at –0.4 volts: ~0.7mS/cm^2 for REF, ~1.0mS/cm^2 for F1 and ~1.1mS/cm^2 for F2. The 50% difference in these values is supported by the general trend of the data in Figure 7 and shows that the shunt conductance is higher in modules F1 and F2.

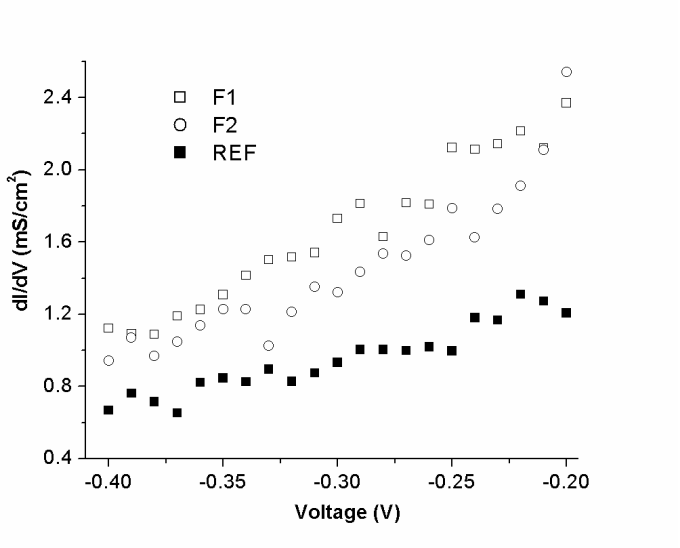

Figure 7. *Average value of dI/dV at far reverse bias for samples from modules F1, F2 and REF. A precise value for the shunt conductance can not be determined, but dI/dV is approximately 50% larger for F1 and F2 than for REF at –0.4V.*

To gain more insight into the observed IV-behaviour of the samples, CV-measurements in the dark were used to evaluate the apparent doping concentration in the absorber as a function of distance from the junction. Apparent doping concentration N at a distance W from the junction was calculated from

$$N(W) = C^3 (q\varepsilon \frac{dC}{dV})^{-1} \qquad (1)$$

where C is the capacitance, V the voltage, q the elementary charge and ε the permittivity. A value of 8.91 was used for the relative permittivity of polycrystalline CdTe [14]. The distance from the junction was calculated from W = ε / C(V). The resulting average doping profiles for samples from each module are shown in Figure 8. While the absolute values of doping concentration are subject to the uncertainties of using the CV-profiling method in thin-film solar cells [15], a relative comparison shows that module F1 has a wider depletion region than REF while the F2 profile is almost identical to REF. A wider depletion region corresponds to a weaker electric field which reduces charge-carrier collection and decreases FF and V_{OC}. This degradation mechanism thus explains part of the degradation observed in module F1.

Finally, to distinguish between the degradation modes $\mathbf{R_{TCO}}$ and **Cell**, a separate comparison of the relative magnitude of R_{TCO} for the different samples was done by placing a measurement contact on the opposite side of the active region from contact D in Figure 1. The measured resistance was that of the TCO layer under the active region with two 8.5mm wide contacts at a distance of 10mm from each other. Table 3 shows the average resistance for each module, where error limits are the standard deviation between the samples. It can be concluded that R_{TCO} is 6% larger in F1 and 9% larger in F2 than in REF, although the differences fall within the limits of error.

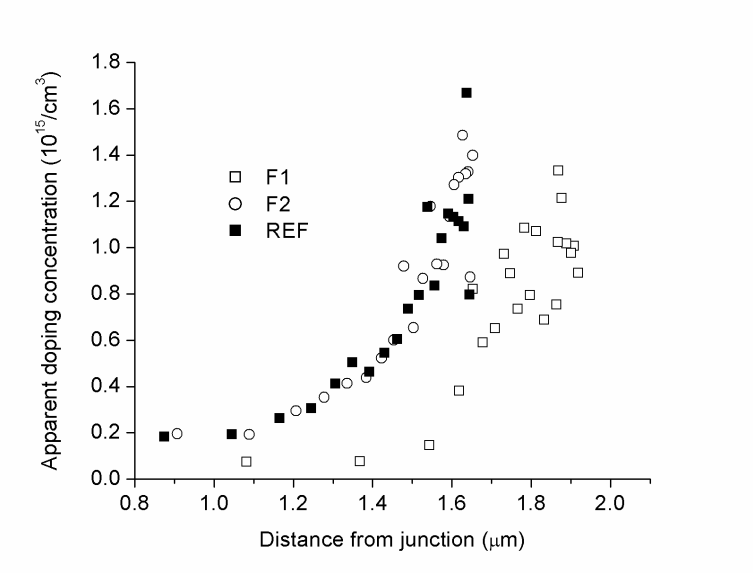

Figure 8. *Average CV doping profiles for modules F1, F2 and REF. The increase in apparent doping concentration in modules F2 and REF occurs closer to the junction than in F1, indicating that F1 has a wider depletion region.*

Table 3*: Resistance below active area (proportional to R_{TCO}) for each module*

Module	R (Ω)
F1	13.6 ± 2.1
F2	14.0 ± 1.5
REF	12.8 ± 1.3

3.3.3. Modeling of degradation impact

To evaluate the relative impact of the degradation modes **R_{TCO}** and **Cell** in this study, as well as the impact of the different degradation mechanisms which belong to the **Cell** degradation mode, a two-diode circuit was used to model the REF curve in Figure 6. An opposing diode was added to the normal solar cell equivalent circuit to give the circuit shown in Figure 9. When the current I is negative, the IV-equation for this circuit becomes

$$V = V_1 + V_2 + V_3 = \frac{A_1 kT}{q} \ln\left(\frac{I + I_L - GV_1}{I_{01}} + 1\right) - \frac{A_2 kT}{q} \ln\left(1 - \frac{I}{I_{02}}\right) - |I| R_S \,, \qquad (2)$$

where V_1 and V_2 are the voltages over the two diodes, V_3 is the resistive voltage loss which is negative irrespective of the direction of the current, A_1 and A_2 are the quality factors of the diodes, I_{01} and I_{02} their saturation currents, and G is the shunt

conductance. The parameters of equation 2 were approximated by performing a least-squares fit to the average D-E IV-curve of the REF samples. The resulting model curve is compared to the REF curve in Figure 10, and the corresponding parameter values are shown in Table 4. The degradation in R_{TCO} and dI/dV was simulated by varying the model parameters G and R_S. A 10% increase in R_S caused a relative FF loss of 4.0%, while a 50% increase in G resulted in a relative FF loss of 0.5%. Increased TCO resistance thus explains part of the FF degradation in both modules F1 and F2.

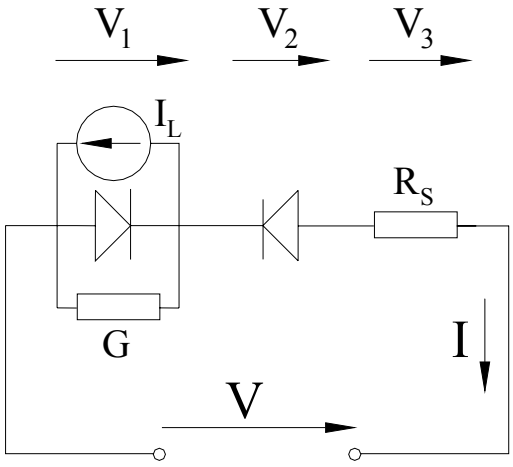

Figure 9. *Equivalent circuit including a reverse-biased back contact diode, used for modeling the IV-behaviour of the samples.*

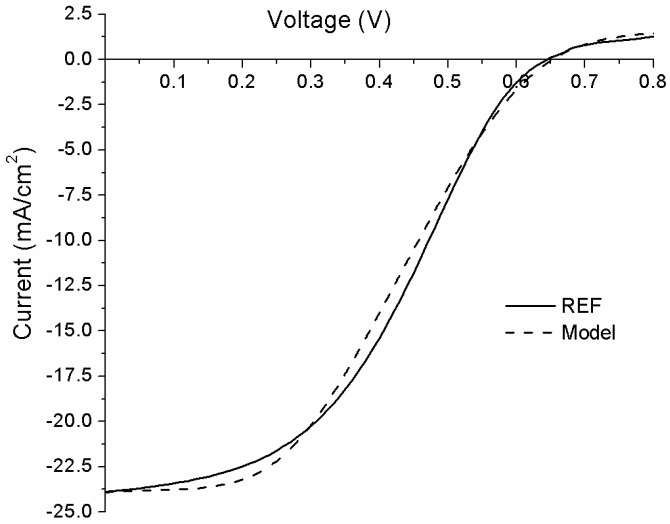

Figure 10. *Average sample IV-curve for module REF measured from contacts D-E, and the corresponding two-diode model curve calculated with a least-squares fit.*

***Table 4**: Parameters in equation 2 after fitting.*

Parameter	A_1	A_2	I_{01} (mA/cm^2)	I_{02} (mA/cm^2)	G (mS/cm^2)	I_L (mA/cm^2)	R_S (Ωcm^2)
Value	1.5	2.0	$9.4 \cdot 10^{-7}$	1.6	0.82	24.2	7.0

4. Discussion

The results in this study show that the decrease in fill factor which was found in module F1 can be at least partly explained by a decreased doping level close to the junction and increased resistance in the TCO layer. In module F2, the doping levels did not change, but FF degradation can be partly attributed to increased TCO resistance. Increased shunt conductance in the cell and across interconnect 1 was also observed in both modules, but they have only a minor effect on the IV-curve. In general, the degradation results from small-sample measurements presented in Table 2 correspond only partially with the field-test results presented in Figure 3. Possible explanations for this are that the number of measured samples was too small to cover spatial variations within the module or that degradation mechanisms which could not be observed in small samples contributed to module degradation.

The degradation mechanisms found in the small samples can not be considered all-inclusive even though they are reliable indicators of module degradation. If problem cells could be located in the module before cutting of the samples, the accuracy of the results would improve significantly. The similarity between the field degradation observed in this study and the accelerated ageing degradation observed in [6] may give information on the stress factors which contributed to decreased field performance. In [6], accelerated ageing was performed in light-soaking and open-circuit conditions, and field tested modules in this study were in open-circuit except during IV-scanning. Open-circuit conditions have been found to be most conducive to cell degradation during accelerated ageing also for other CdTe cell types [16,17]. The results in this study indicate that bias light or voltage should be included as a stress factor when the field lifetime of modules of this type is estimated with accelerated ageing experiments. Unfortunately, further accelerated ageing tests could not be undertaken within this study.

5. Conclusions

The field-tested CdTe modules in this study showed significant degradation in maximum power during one and a half years outdoors, primarily because of decreased FF and V_{OC}. Samples cut from the modules showed the same degradation effects in the measurement of a small active area, although the small number of samples limited the accuracy by which sample averages mirrored outdoor test results. Multi-contact measurements revealed that significant degradation could not be attributed to the cell interconnects, leaving the active cell material and the front contact TCO as the only possible sources of degradation. Compared to the reference module samples, the samples from the field tested modules F1 and F2 showed a smaller rollover at far

forward bias and degradation in FF. The degradation mechanisms behind this performance loss were identified as decreased dopant concentration close to the junction and increased series resistance in the TCO. We note the similarity of the degradation modes found in this study to those reported in [6] for CdTe cells with back and front contact structures similar to the ones studied here. Damp-heat ageing of mini-modules in this study showed that the module structure is not sensitive to moisture and is stable in heat.

This study is a step towards lifetime prediction for CdTe modules. The general conclusion which can be drawn from this work is: Some, but not all, cell-level degradation mechanisms which occur in the field can be identified by the electrical characterization of small-area representative samples after the removal of the encapsulation. In this study, processes causing FF degradation in small-area samples are believed to have caused degradation in FF also at the module level, whereas the lower current density of a large module makes the analysis of current degradation less straightforward and an analysis of voltage degradation would have required a larger number of samples. The specific conclusion for the CdTe technology studied in this work is that detailed lifetime estimates may require the inclusion of bias light or voltage in accelerated ageing experiments to elucidate the degradation mechanisms which occur in the field.

Acknowledgements
Svenska Litteratursällskapet i Finland rf and Magnus Ehrnrooths stiftelse are thanked for financial support.

References

1. McMahon T. Accelerated testing and failure of thin-film PV modules. *Progress in Photovoltaics: Research and Applications* 2004; **12** (2-3): 235-248. DOI: 10.1002/pip.526

2. Dobson K, Visoly-Fisher I, Hodes G, Cahen D. Stability of CdTe/CdS thin-film solar cells. *Solar Energy Materials & Solar Cells* 2000; **62**(3): 295-325.

3. Visoly-Fisher I, Dobson K, Nair J, Bezalel E, Hodes G, Cahen D. Factors affecting the stability of CdTe/CdS solar cells deduced from stress tests at elevated temperature. *Advanced Functional Materials* 2003; **13** (4): 289-299. DOI: 10.1002/adfm.200304259

4. Roschier S. *Development of procedures for performance measurements and lifetime testing of thin film photovoltaic devices.* Doctoral dissertation. Helsinki University of Technology, 2002.

5. Bätzner D, Romeo A, Terheggen M, Döbeli M, Zogg H, Tiwari A. Stability aspects in CdTe/CdS solar cells. *Thin Solid Films* 2004; **451-452**: 536-543. DOI: 10.1016/j.tsf.2003.10.141

6. Degrave S, Nollet P, Stojanoska G, Burgelman M, Durose K. Interpretation of ageing experiments on CdTe/CdS solar cells. *Proceedings of the 17th European Photovoltaic Solar Energy Conference,* 2001; 1058-1061.

7. Mrig L, Rummel S. Outdoor stability of performance of CIS and CdTe photovoltaic modules at SERI. *Proceedings of the 21st IEEE PV Specialist Conference*, 1990; 1038-1039.

8. del Cueto J. Review of the field performance of one cadmium telluride module. *Progress in Photovoltaics: Research and Applications* 1998; **6** (6): 433-446.

9. Ullal H, Zweibel K, von Roedem B. Current status of polycrystalline thin-film PV technologies. *Proceedings of the 26th IEEE PV Specialists Conference*, 1997; 301-305.

10. Czanderna A, Jorgensen G. Accelerated life testing and service lifetime prediction for PV technologies in the twenty-first century. *Electrochemical Society Proceedings 99-11 (Photovoltaics for the 21st century)* 1999; 57-67.

11. Mohring H-D, Stellbogen D, Schäffler R, Oelting S, Gegenwart R, Konttinen P, Carlsson T, Cendagorta M, Herrmann W. Outdoor performance of polycrystalline thin film PV modules in different European climates. *Proceedings of the 19thEuropean Photovoltaic Solar Energy Conference*, 2004; 2098-2101.

12. McMahon T, Fahrenbruch A. Insights into the non-ideal behaviour of CdS/CdTe solar cells. *Proceedings of the 28th IEEE PV Specialists Conference*, 2000; 539-542.

13. Burgelman M, Nollet P, Degrave S, Beier J. Modeling the cross-over of the I-V-characteristics of thin film CdTe solar cells. *Proceedings of the 28th IEEE PV Specialists Conference*, 2000; 551-554.

14. El-Kadry N, Ashour A, Mahmoud S. Structural dependence of d.c. electrical properties of physically deposited CdTe thin films. *Thin Solid Films* 1995; **269**: 112-116.

15. Hegedus S, Shafarman W. Thin-film solar cells: Device measurement and analysis. *Progress in Photovoltaics: Research and Applications* 2004; **12** (2-3): 155-176. DOI: 10.1002/pip.518

16. Hiltner J, Sites J. Stability of CdTe solar cells at elevated temperatures: bias, temperature and Cu dependence. *AIP Conference Proceedings* 1999; **462**: 170-175.

17. Powell R, Sasala R, Rich G, Steele M, Bihn K, Reiter N, Cox S, Dorer G. Stability testing of CdTe/CdS thin-film photovoltaic modules. *Proceedings of the 25th IEEE PV Specialists Conference*, 1996; 785-788.